Predictability of the coherent-noise model and its applications

N. V. Sarlis* and S.-R. G. Christopoulos
Solid State Section and Solid Earth Physics Institute, Physics Department, University of Athens, Panepistimiopolis, Zografos 157 84, Athens, Greece

(Received 21 February 2012; revised manuscript received 26 April 2012; published 25 May 2012)

We study the threshold distribution function of the coherent-noise model for the case of infinite number of agents. This function is piecewise constant with a finite number of steps n. The latter exhibits a $1/f$ behavior as a function of the order of occurrence of an avalanche and hence versus natural time. An analytic expression of the expectation value $\mathscr{E}(S)$ for the size S of the next avalanche is obtained and used for the prediction of the next avalanche. Apart from $\mathscr{E}(S)$, the number of steps n can also serve for this purpose. This enables the construction of a similar prediction scheme which can be applied to real earthquake aftershock data.

DOI: 10.1103/PhysRevE.85.051136 PACS number(s): 05.40.−a, 05.45.Tp, 89.75.Da, 91.30.Dk

I. INTRODUCTION

The appearance of scale-free behavior in dynamical systems operating far from equilibrium has been reported in a large variety of cases ranging from biology [1–5] to seismology [6–10], and from solar flares [11–14] to rice piles [15–17] and electric signals that precede rupture [18]. An explanation of the ubiquity of scale invariance in nature has been attempted [19–21] in terms of the self-organized criticality (SOC) concept originally suggested by Bak, Tang, and Wiesenfeld [22]. Self-organized critical dynamical systems usually contain many agents which interact under the influence of a slow driving force. The rearrangements induced lead, after a transient during which the system acquires criticality [23,24], to a stationary state which is characterized by power laws without the need for fine tuning an external parameter. Thus, in SOC systems, the competition between a driving force that very slowly injects energy and the interactions between the agents can drive the system into a critical state where a minor perturbation can trigger an avalanche of any size and duration [22,25,26]. As suggested by Newman and Sneppen [5,27,28], however, power-law behavior can also be triggered when imposing *coherently* (that means at the same time) to all agents an external, probably environmental, stress of stochastic origin, such as noise, and assume the agents as noninteracting. Since the agents are noninteracting such a coherent noise model cannot be considered as critical although it gives rise to power laws. The coherent noise model as suggested in Refs. [27,28] has already found useful applications for both earthquakes [5,28–30] and scale-free dynamical systems in general [31,32].

Scale-free dynamical systems usually give rise to strong avalanches, e.g., strong earthquakes in seismology, whose prediction poses a very important problem [23,24,26,33–45]. For the case of critical systems, including SOC, we expect that such strong avalanches emerge when the system approaches a critical state, e.g., see Ref. [46]. The approach of a system to a critical state can be identified (e.g., see Ref. [47]) by using the concept of natural time analysis [46,48,49]. However, in the case of the coherent noise model [27,28] since the system is noncritical, a challenge emerges as to whether its avalanches can be predicted.

In a time series comprising N avalanches the *natural time* $\chi_k = k/N$ serves as an index [48,50] for the occurrence of the kth avalanche. The avalanches in the coherent noise model result from the following procedure [27,28]: Consider a system of N_a agents, e.g., points of contact in a fault. For each agent i we associate a threshold x_i, $i = 1,2,\ldots,N_a$, that represents the amount of stress that the agent withstands before it moves. Without loss of generality [27,28], x_i may come from the uniform distribution in the interval $0 \leqslant x < 1$. The dynamics of the model consists of two steps, a "stress" step, which is more important and sufficient to produce large avalanches, and an "aging" step. During the stress step, we select a random number (or stress level) η from some probability distribution function $p_{\text{stress}}(\eta)$ and replace all x_i that are smaller than η with new values resulting from the uniform distribution in the interval $0 \leqslant x < 1$. The number of agents whose thresholds are renewed is the size S of the avalanche. During the aging step, a fixed fraction f of agents is selected at random and their thresholds are also replaced with new thresholds resulting again from the uniform distribution in the interval $0 \leqslant x < 1$. If we assume that $N_a \to \infty$, the thresholds x_i are represented by a threshold distribution function $p_{\text{thres}}(x)$, which initially ($k = 0$) is considered uniform in the interval $0 \leqslant x < 1$, i.e., $p^{(0)}_{\text{thres}}(x) = 1$. The size S_1 of the first avalanche ($k = 1$) is just the probability $\text{Prob}[x < \eta_1] = \int_0^{\eta_1} p^{(0)}_{\text{thres}}(x)dx = \eta_1$, which represents the "mass" of the agents that had thresholds smaller than η_1. After the subsequent aging step the threshold distribution becomes $p^{(1)}_{\text{thres}}(x)$. When repeating the two steps for the second time—using η_2— we can obtain S_2 and $p^{(2)}_{\text{thres}}(x)$ and so on. As we shall show below in Sec. II, the threshold distribution function after the kth avalanche $p^{(k)}_{\text{thres}}(x)$ is a piecewise constant function with a finite number of steps n_k. This number n_k has been studied in a different context in natural time [51] and shown to exhibit a $1/f$ behavior.

In this paper, we will focus on the predictability of the coherent noise model in view of the knowledge accumulated from natural time analysis [46]. The paper is organized as follows: In Sec. II, we discuss some properties of $p^{(k)}_{\text{thres}}(x)$ and based on its knowledge we derive an analytic expression of the expectation value $\mathscr{E}(S_{k+1})$ for the size S_{k+1} of the next avalanche in the case [27,30–32] of an exponentially

*Corresponding author: nsarlis@phys.uoa.gr

distributed coherent noise, i.e., $p_{\rm stress}(\eta) = \exp(-\eta/\sigma)/\sigma$. In Sec. III, we present our results on the predictability of the coherent noise model based on $\mathscr{E}(S_{k+1})$. The possible application of these results to real earthquake data is discussed in Sec. IV and the conclusions are presented in Sec. V.

II. THE COHERENT-NOISE MODEL FOR AN INFINITE NUMBER OF AGENTS

As already mentioned, when the number of agents is infinite ($N_a \to \infty$) the stresses x_i of the agents are replaced by a threshold distribution function $p_{\rm thres}(x)$ defined in the interval $0 \leqslant x < 1$. As stated by Newman and Sneppen [27], this function can be determined in a formally exact way during the evolution of the model. The way used in the present study is the following: Before the first avalanche, i.e., at $k = 0$,

$$p^{(0)}_{\rm thres}(x) = 1. \tag{1}$$

When the first coherent stress is applied, the random number η_1 eliminates all probability mass below η_1, giving rise to an avalanche of size

$$S_1 = \int_0^{\eta_1} p^{(0)}_{\rm thres}(x)dx = \eta_1. \tag{2}$$

This mass S_1 is then redistributed uniformly in the interval $0 \leqslant x < 1$ and the threshold distribution becomes

$$\left[p^{(0)}_{\rm thres}(x)\right]' = S_1 + \Theta(x-\eta_1)p^{(0)}_{\rm thres}(x), \tag{3}$$

where $\Theta(x)$ is the Heaviside (unit) step function, i.e., $\Theta(x) = 0$ if $x < 0$ and $\Theta(x) = 1$ if $x \geqslant 0$. Later, the aging step is applied reducing $[p^{(0)}_{\rm thres}(x)]'$ by a fraction $(1-f)$, since $[p^{(0)}_{\rm thres}(x)]'$ is normalized to unity, and redistributing uniformly a mass of probability f. Thus, after the first avalanche we have

$$p^{(1)}_{\rm thres}(x) = (1-f)\left[p^{(0)}_{\rm thres}(x)\right]' + f, \tag{4}$$

leading to

$$p^{(1)}_{\rm thres}(x) = [(1-f)\eta_1 + f] + (1-f)\Theta(x-\eta_1), \tag{5}$$

which is schematically shown in Fig. 1(a).

When the second random stress η_2 is applied, an equivalent of Eq. (3) holds:

$$\left[p^{(1)}_{\rm thres}(x)\right]' = S_2 + \Theta(x-\eta_2)p^{(1)}_{\rm thres}(x), \tag{6}$$

where

$$\begin{aligned} S_2 &= \int_0^{\eta_2} p^{(1)}_{\rm thres}(x)dx \\ &= [(1-f)\eta_1 + f]\eta_2 + (1-f)(\eta_2-\eta_1)\Theta(\eta_2-\eta_1). \end{aligned} \tag{7}$$

Then, the aging step transforms the threshold density of Eq. (6), according to

$$p^{(2)}_{\rm thres}(x) = (1-f)\left[p^{(1)}_{\rm thres}(x)\right]' + f. \tag{8}$$

The application of Eqs. (6) and (8) for the threshold density of Eq. (5), may lead to two functional forms for $p^{(2)}_{\rm thres}(x)$ depending on whether η_2 is smaller or larger than η_1. When $\eta_2 < \eta_1$, see Fig. 1(b), Eq. (8) becomes

$$\begin{aligned} p^{(2)}_{\rm thres}(x) = {} & [f + f(1-f)\eta_2 + (1-f)^2\eta_2\eta_1] \\ & + [f(1-f) + (1-f)^2\eta_1]\Theta(x-\eta_2) \\ & + (1-f)^2\Theta(x-\eta_1), \end{aligned} \tag{9}$$

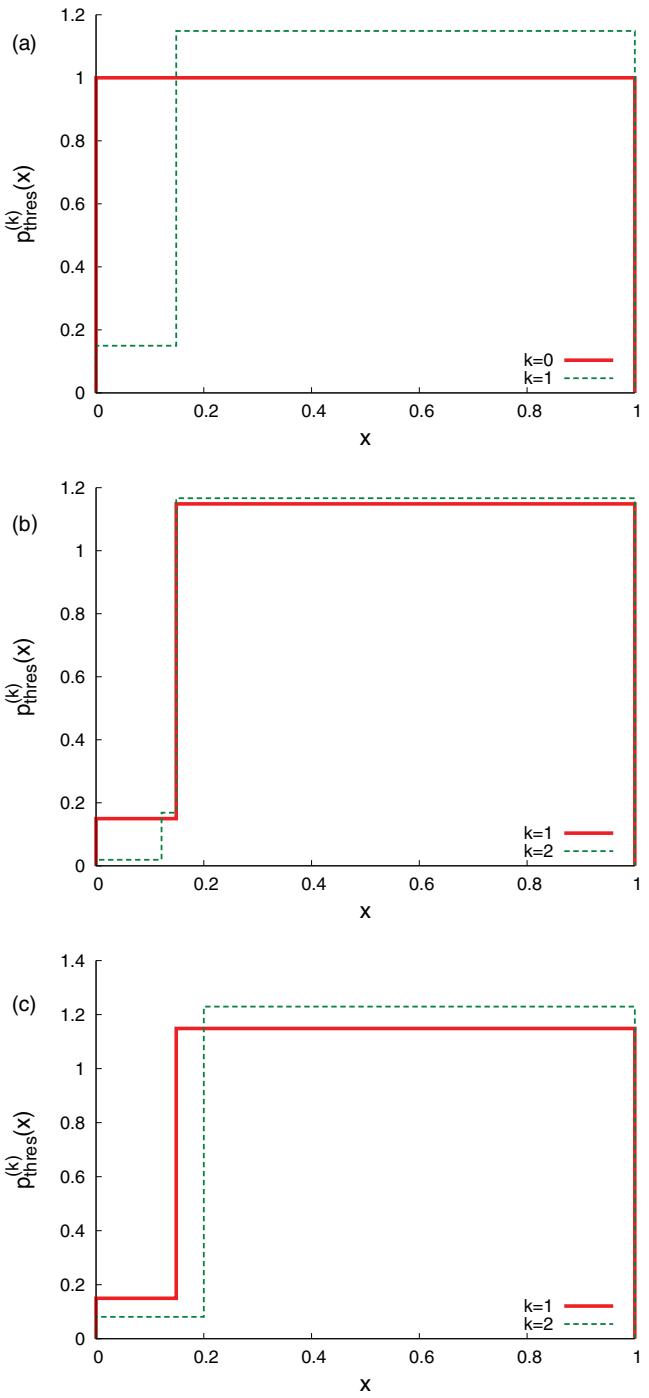

FIG. 1. (Color online) The threshold distribution function $p^{(k)}_{\rm thres}(x)$ of the coherent-noise model when the number of agents is infinite after the k-th avalanche for (a) $k = 1$, (b) $k = 1$ and $k = 2$ when $\eta_2 < \eta_1$, and (c) $k = 1$ and $k = 2$ when $\eta_2 > \eta_1$. The case $k = 0$, i.e., before the first avalanche, is also shown in panel (a).

whereas for $\eta_2 > \eta_1$ [see Fig. 1(c)], it leads to

$$\begin{aligned} p^{(2)}_{\rm thres}(x) = {} & [f + f(1-f)\eta_2 + (1-f)^2(\eta_2\eta_1 + \eta_2 - \eta_1)] \\ & + [(1-f) + (1-f)^2\eta_1]\Theta(x-\eta_2). \end{aligned} \tag{10}$$

The expressions of Eqs. (5), (9), and (10) for the threshold distribution function though lengthy, can be written in the

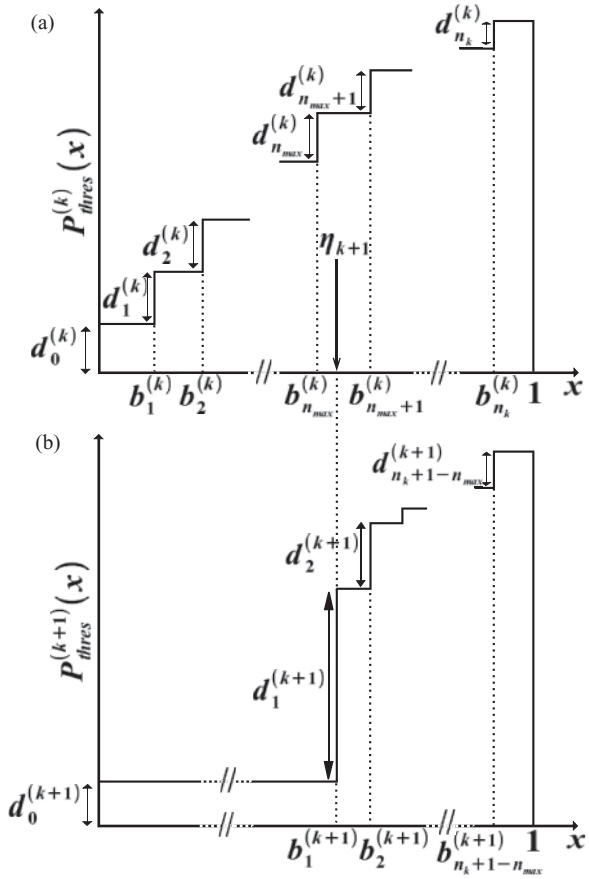

FIG. 2. Schematic diagram of the transformation of $p^{(k)}_{\rm thres}(x)$ upon the occurrence of the $k+1$-th avalanche

following general form:

$$p^{(k)}_{\rm thres}(x) = \sum_{n=0}^{n=n_k} d^{(k)}_n \Theta\big(x - b^{(k)}_n\big), \tag{11}$$

where n_k is the number of *steps* present in the threshold distribution function after the kth avalanche and $b^{(k)}_0 = 0$, leading to $\Theta(x) \equiv 1$ for the interval $0 \leqslant x < 1$, where $p^{(k)}_{\rm thres}(x)$ is defined. When $k = 1$, for example, $n_1 = 1$ with $d^{(1)}_0 = (1-f)\eta_1 + f$, $b^{(1)}_0 = 0$, $d^{(1)}_1 = 1 - f$, and

$$b^{(1)}_1 = \eta_1 \tag{12}$$

[see Eq. (5) and Fig. 1(a)].

Equation (11) allows the determination of $p^{(k+1)}_{\rm thres}(x)$ once η_{k+1} has been selected (see Fig. 2). The size $S_{k+1} = \int_0^{\eta_{k+1}} p^{(k)}_{\rm thres}(x)dx$ is given by

$$S_{k+1} = \sum_{n=0}^{n=n_k} d^{(k)}_n \big(\eta_{k+1} - b^{(k)}_n\big)\Theta\big(\eta_{k+1} - b^{(k)}_n\big), \tag{13}$$

the stress step leads to

$$\big[p^{(k)}_{\rm thres}(x)\big]' = S_{k+1} + \Theta(x - \eta_{k+1})p^{(k)}_{\rm thres}(x), \tag{14}$$

and the aging step to

$$p^{(k+1)}_{\rm thres}(x) = (1-f)\big[p^{(k)}_{\rm thres}(x)\big]' + f. \tag{15}$$

Let $n_{\max}$ be the maximum integer such that

$$b^{(k)}_{n_{\max}} < \eta_{k+1} < b^{(k)}_{n_{\max}+1}, \tag{16}$$

if $\eta_{k+1} > b^{(k)}_{n_k}$, then $n_{\max} = n_k$. Then, Eqs. (11), (13), (14), and (15) lead to

$$\begin{aligned}
&b^{(k+1)}_0 = 0, \quad d^{(k+1)}_0 = (1-f)S_{k+1} + f,\\
&b^{(k+1)}_1 = \eta_{k+1}, \quad d^{(k+1)}_1 = (1-f)\left(\sum_{n=0}^{n_{\max}} d^{(k)}_n\right),\\
&b^{(k+1)}_2 = b^{(k)}_{n_{\max}+1}, \quad d^{(k+1)}_2 = (1-f)d^{(k)}_{n_{\max}+1},\\
&b^{(k+1)}_3 = b^{(k)}_{n_{\max}+2}, \quad d^{(k+1)}_3 = (1-f)d^{(k)}_{n_{\max}+2},\\
&\qquad \ldots, \quad \ldots\\
&b^{(k+1)}_{n_{k+1}} = b^{(k)}_{n_k}, \quad d^{(k+1)}_{n_{k+1}} = (1-f)d^{(k)}_{n_k},
\end{aligned} \tag{17}$$

where $n_{k+1} = n_k - n_{\max} + 1$. All the above equations are valid as far as η_{k+1} is smaller than unity. If $\eta_{k+1} > 1$, then obviously

$$S_{k+1} = 1 \tag{18}$$

and

$$p^{(k+1)}_{\rm thres}(x) = p^{(0)}_{\rm thres}(x), \tag{19}$$

with

$$d^{(k+1)}_0 = 1, \quad b^{(k+1)}_0 = 0, \tag{20}$$

and the system has been completely *regenerated*.

Thus, Eq. (11) together with either Eq. (17) or Eq. (19) describe the evolution of the threshold distribution function of the coherent-noise model in the case of infinite agents. The evolution of the system as k increases is reflected in the change of the $2n_k$ quantities $b^{(k)}_n, d^{(k)}_n$ for $n = 1,2,\ldots,n_k$, because $b^{(k)}_0 = 0$ and

$$d^{(k)}_0 = 1 - \sum_{n=1}^{n_k} d^{(k)}_n \big(1 - b^{(k)}_n\big), \tag{21}$$

due to the normalization condition of the threshold distribution function $p^{(k)}_{\rm thres}(x)$. The quantity n_k is itself a random variable (see Fig. 3) resulting from η_l, $l = 1,2,\ldots,k$. Its properties will be later discussed in detail in Sec. IV.

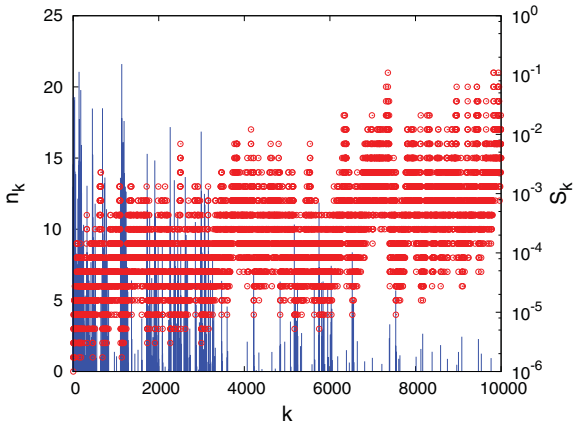

FIG. 3. (Color online) Example of the evolution of the quantity n_k (red circles, left scale) after the k-th avalanche for $\sigma = 0.05$ and $f = 10^{-7}$. The avalanche sizes S_k (blue impulses, right scale) are also shown.

The knowledge of the $2n_k$ quantities $b_n^{(k)}, d_n^{(k)}$ for $n = 1,2,\ldots,n_k$, enables the exact calculation of the probability distribution $p(S_{k+1})$ of the next avalanche S_{k+1}. This is so because

$$p(S_{k+1}) = \int_0^\infty p(S_{k+1}|\eta) p_{\text{stress}}(\eta) d\eta, \tag{22}$$

where $p(S_{k+1}|\eta)$ is [27] the conditional probability to have an avalanche of size S_{k+1} given that $\eta_{k+1} = \eta$. Due to Eqs. (13) and (18), this conditional probability is given by

$$p(S_{k+1}|\eta) = \delta\left\{ S_{k+1} - \min\left[\sum_{n=0}^{n=n_k} d_n^{(k)} \left(\eta - b_n^{(k)}\right) \Theta\left(\eta - b_n^{(k)}\right), 1 \right] \right\}, \tag{23}$$

where $\delta(x)$ is the Dirac's delta distribution and $\min(x,y)$ stands for the minimum of x and y. Substituting Eq. (23) into Eq. (22), we obtain

$$p(S_{k+1}) = \sum_{l=0}^{n_k} \int_{b_l^{(k)}}^{b_{l+1}^{(k)}} \delta\left[S_{k+1} - \sum_{n=0}^{n=l} d_n^{(k)} \left(\eta - b_n^{(k)}\right) \right] p_{\text{stress}}(\eta) d\eta + \delta(S_{k+1} - 1) \int_1^\infty p_{\text{stress}}(\eta) d\eta \tag{24}$$

where $b_{n_k+1}^{(k)} = 1$. Using now the definitions

$$\alpha_l \equiv \sum_{n=0}^{l} d_n^{(k)}, \quad \beta_l \equiv \sum_{n=0}^{l} d_n^{(k)} b_n^{(k)}, \tag{25}$$

and the properties of Dirac's δ distribution, we finally obtain

$$p(S_{k+1}) = \sum_{l=0}^{n_k} \frac{\Theta\left(S_{k+1} - \alpha_l b_l^{(k)} + \beta_l\right) \Theta\left(\alpha_l b_{l+1}^{(k)} - \beta_l - S_{k+1}\right)}{\alpha_l} \times p_{\text{stress}}\left(\frac{S_{k+1} + \beta_l}{\alpha_l} \right) + \delta(S_{k+1} - 1) \int_1^\infty p_{\text{stress}}(\eta) d\eta. \tag{26}$$

Equation (26) allows the determination of the exact size distribution of the next $k+1$th avalanche given the $2n_k$ quantities $b_n^{(k)}, d_n^{(k)}$ for $n = 1,2,\ldots,n_k$ and the stress distribution $p_{\text{stress}}(\eta)$. In the commonly used [27,30–32] case that $p_{\text{stress}}(\eta) = \exp(-\eta/\sigma)/\sigma$, the expectation value

$$\mathscr{E}(S_{k+1}) \equiv \int_0^\infty S_{k+1} p(S_{k+1}) d S_{k+1} \tag{27}$$

of the size S_{k+1} results in (see Appendix A)

$$\mathscr{E}(S_{k+1}) = \sigma \sum_{l=0}^{n_k} d_l^{(k)} \left[\exp\left(-\frac{b_l^{(k)}}{\sigma}\right) - \exp\left(-\frac{1}{\sigma}\right) \right]. \tag{28}$$

III. THE PREDICTABILITY OF THE COHERENT-NOISE MODEL

Since Eq. (28) provides an analytic expression for the expected size $\mathscr{E}(S_{k+1})$ of the next $k+1$th avalanche, we investigate whether $\mathscr{E}(S_{k+1})$ can be used as a decision variable for binary "predictions" in the sense described in Ref. [23] (see also Ref. [52]). We note that in the latter reference the decision variable and the prediction based on it requires training a conditional probability from half the data set. The approach we follow here is less elaborated since we make use of the analytic study of the previous section and directly apply Eq. (28) for the expected size $\mathscr{E}(S_{k+1})$. Thus, we run the coherent-noise model described by Eqs. (11), (13), (17), and/or (20) for the first $k = 10^6$ avalanches and after each avalanche k we estimated $\mathscr{E}(S_{k+1})$. For reasons of convenience, we convert both $\mathscr{E}(S_{k+1})$ and S_{k+1} to their respective "magnitudes" $M'_{k+1} \equiv \log_{10}[\mathscr{E}(S_{k+1})]$ and $M_{k+1} \equiv \log_{10}(S_{k+1})$. The time increased probability (TIP) [53,54] is turned on when $M'_{k+1} \geqslant M_c$, where M_c is a given threshold in the prediction. If the magnitude M_{k+1} of the next avalanche is greater than or equal to a target avalanche magnitude threshold M_{target}, we have a successful prediction. For binary predictions, the prediction of events becomes a classification task with two types of errors: missing an event and giving a false alarm. We therefore choose [23] the receiver operating characteristics (ROC) graph [55] to depict the prediction quality. This is a plot of the hit rate versus the false alarm rate, as a function of the total rate of alarms, which is tuned by the threshold M_c [55]. The hit rate (or true positive rate) is the ratio of the cases for which TIP was on and $M_{k+1} \geqslant M_{\text{target}}$ over the total number of cases that $M_{k+1} \geqslant M_{\text{target}}$. The false alarm rate (or false positive rate, FPR) is the ratio of the cases for which TIP was on and $M_{k+1} < M_{\text{target}}$ over the total number of cases for which $M_{k+1} < M_{\text{target}}$. Only if in between the hit rate exceeds the false alarm rate, is the predictor useful. Random predictions generate equal hit and alarm rates, and hence they lead to the diagonal in a ROC plot. Thus, only when the points lie above this diagonal is the predictor useful. As an example, the ROC graph for $\sigma = 0.05$ and $f = 10^{-7}$ is shown in Fig. 4. For

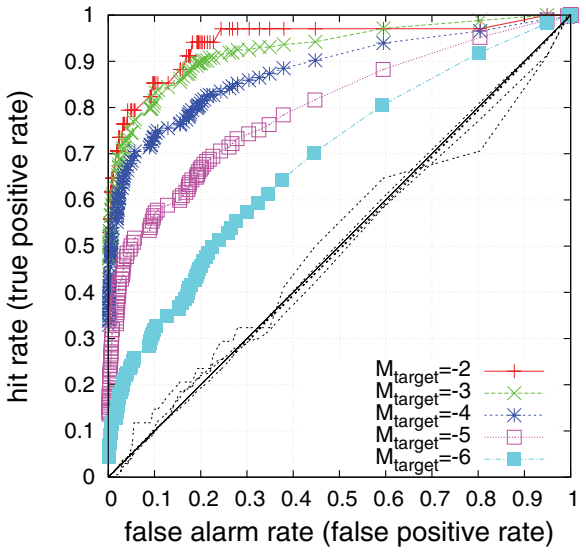

FIG. 4. (Color online) Receiver Operating Characteristics when using $\mathscr{E}(S_{k+1})$ as a predictor (lines with symbols) for the coherent-noise model with $\sigma = 0.05$ and $f = 10^{-7}$ for the first 10^6 avalanches. They correspond to $M_{\text{target}} = -6, -5, -4, -3$, and -2 from the bottom to the top at FPR = 20%. The results of the same calculation when $\mathscr{E}(S_{k+1})$ have been randomly shuffled are also shown (grey broken lines without symbols).

every given threshold value M_c and a target threshold M_{target}, we get a point in this plot, thus by varying M_c we get a curve. The various curves in Fig. 4 correspond to various values of $M_{\text{target}} = -6, -5, \ldots, -2$ increasing from the bottom to the top at FPR = 20%. Since the points in each curve lie above the diagonal, we see that $\mathscr{E}(S_{k+1})$ exhibits predictive power that increases for larger values of M_{target}. In order to investigate the statistical validity of this result, we include in the same graph the results when the values of $\mathscr{E}(S_{k+1})$ have been shuffled; we obtain curves which are close to the diagonal, thus the predictive power of $\mathscr{E}(S_{k+1})$ cannot be considered as chancy.

IV. DISCUSSION AND APPLICATIONS

The exact knowledge of the threshold distribution $p^{(k)}_{\text{thres}}(x)$ for a real system like a fault is impossible (for example, see pp. 358–362 of Ref. [46], where the possibility of predicting large avalanches in the Olami-Feder-Christensen earthquake model [56] has been discussed; see also Ref. [57]). Thus, even if active faults followed the coherent-noise model (but see also the last paragraph of this section), the application of the prediction scheme of Sec. III would be practically impossible. The coherent-noise model, however, captures real aftershock properties (e.g., see Refs. [27,29,30]), and hence it is worthwhile to investigate the results of Sec. II for the presence of an experimentally measurable quantity to predict its avalanches in the sense suggested in Sec. III.

An inspection of Eqs. (11), (26), and (28) points to the relative importance of the number of steps n_k of the threshold distribution function $p^{(k)}_{\text{thres}}(x)$. As mentioned in the Introduction n_k has already been studied [51] in a different context in natural time. In Appendix B, the family of sets E_k of *successive extrema*, defined in Ref. [51], obtained from a given probability distribution function $f(\eta)$ [e.g., $f(\eta) = p_{\text{stress}}(\eta)$] are discussed. The cardinality $\varepsilon_k \equiv |E_k|$ of such sets equals n_k as far as for

$$l = 1,2,\ldots,k, \quad \eta_l < 1. \tag{29}$$

This holds because in this case, due to Eqs. (12) and (17),

$$E_k = \left\{ b^{(k)}_n : 0 < n \leqslant n_k \right\}, \tag{30}$$

and thus $\varepsilon_k = n_k$. It has been shown [51] that ε_k as a function of the natural number k exhibits $1/f^a$ noise with a very close to unity. Moreover, the average value $\langle \varepsilon_k \rangle$ and the variance $\langle (\varepsilon_k - \langle \varepsilon_k \rangle)^2 \rangle$ are given by the following relations [51]:

$$\langle \varepsilon_k \rangle = \sum_{n=1}^{k} \frac{1}{n}, \tag{31}$$

$$\langle (\varepsilon_k - \langle \varepsilon_k \rangle)^2 \rangle = \sum_{n=1}^{k} \left(\frac{1}{n} - \frac{1}{n^2} \right). \tag{32}$$

Equations (31) and (32) reveal that when the condition (29) holds, both the average value and the variance of n_k diverge logarithmically as k tends to infinity. This logarithmic creep signifies that the system ages as k increases. The quantity n_k is shown in Fig. 3 for the first 10 000 avalanches in the case $\sigma = 0.05$ and $f = 10^{-7}$. An inspection of this figure reveals that although the system exhibits aging in the long term—since the

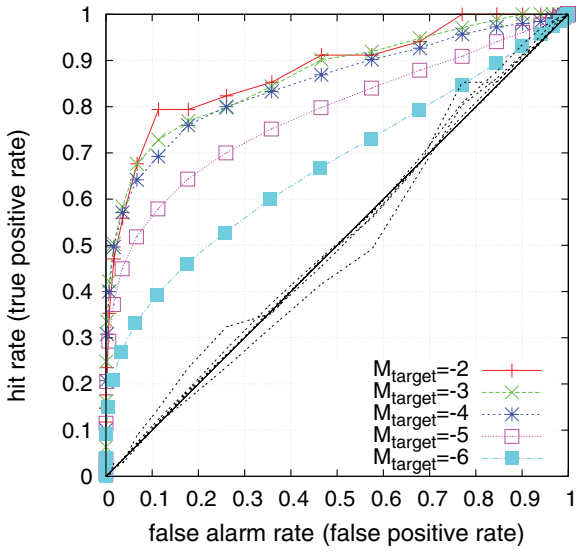

FIG. 5. (Color online) Receiver Operating Characteristics when using n_k as a predictor (lines with symbols) for the coherent-noise model with $\sigma = 0.05$ and $f = 10^{-7}$ for the first 10^6 avalanches. They correspond to $M_{\text{target}} = -6, -5, -4, -3$, and -2 from the bottom to the top at FPR $\approx 47\%$. The results of the same calculation when n_k have been randomly shuffled are also shown (grey broken lines without symbols).

average value of n_k increases—there also exist avalanches that strongly diminish n_k. This occurs when a large η_{k+1} value is selected and—due to Eq. (13)—is accompanied by a relatively large value of S_{k+1}. Thus, a small n_{k+1} value reflects a constant $p^{(k+1)}_{\text{thres}}(x)$ —up to a relatively high value of $\eta_{k+1} (= b^{(k+1)}_1)$— with a large amplitude $d^{(k+1)}_0 = (1-f)S_{k+1} + f$ [cf. Eq. (17), since S_{k+1} is large]. These conditions are favorable for aftershocks [27,29,30]. Thus, when n_k is small we expect "aftershocks" to appear: for example, see close to $k = 5200$ in Fig. 3. Having this in mind, in Fig. 5 we used n_k as a decision variable for the prediction of the first 10^6 avalanches of the coherent-noise model with $\sigma = 0.05$ and $f = 10^{-7}$, i.e., the case treated in Fig. 4. Now, the TIP is on when n_k is smaller than or equal to a threshold n_c which is varied in order to obtain the ROC. We observe that this prediction scheme also has statistically significant predictive power since the red lines with plus symbols in Fig. 5 fall well above the diagonal and above the ROCs obtained when randomly shuffling n_k. Moreover, when comparing Fig. 5 with Fig. 4, we observe that $\mathscr{E}(S_{k+1})$ seems to perform better than n_k. The main advantage, however, is that for real systems, such as earthquakes, we can obtain a rough estimation for n_k from earthquake catalogs.

We now make the assumption that just after the occurrence of a mainshock, Eq. (1) actually describes the points of contact in the subterranean fault as suggested by Newmann and Sneppen [27]. Of course, $p^{(k)}_{\text{thres}}(x)$ cannot be determined, but due to Eqs. (13) and (17) one expects that when a strong aftershock of magnitude m_k occurs it eliminates a large amount of $b^{(k)}_n$'s. Hence, although it is S_k that is actually related with m_k, we could get a crude estimation of n_k by replacing η_k with some simple function of m_k and study the related sets

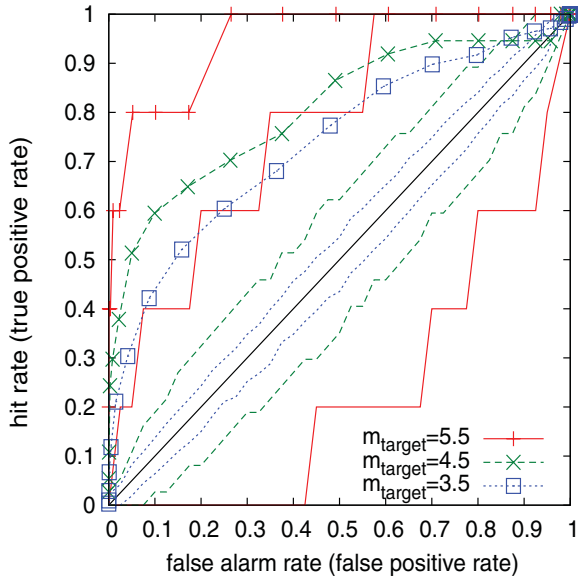

FIG. 6. (Color online) Receiver Operating Characteristics when using ε_k as a predictor for the aftershock sequence of Landers earthquake for target earthquake magnitudes $m_{\text{target}} = 3.5$ (blue squares), 4.5 (green crosses) and 5.5 (red pluses). For each m_{target}, the corresponding broken lines without symbols delimit the 90% central interval in the ROCs obtained from randomly shuffling the original aftershock sequence $\{m_k\}$ and repeating the calculation of ε_k for 10^3 times.

E_k of successive extrema. The applicability of our assumption will become clear once we construct the related ROCs (but see also the next paragraph). In Figs. 6 and 7, we depict

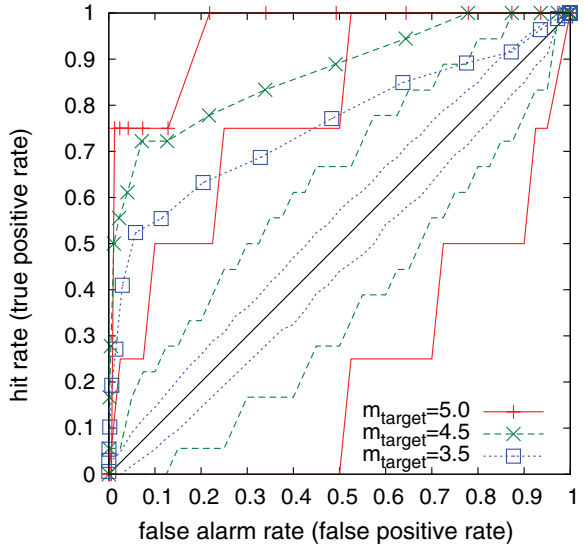

FIG. 7. (Color online) Receiver Operating Characteristics when using ε_k as a predictor for the aftershock sequence of Hector Mine earthquake for target earthquake magnitudes $m_{\text{target}} = 3.5$ (blue squares), 4.5 (green crosses) and 5.0 (red pluses). For each m_{target}, the corresponding broken lines without symbols delimit the 90% central interval in the ROCs obtained from randomly shuffling the original aftershock sequence $\{m_k\}$ and repeating the calculation of ε_k for 10^3 times.

the receiver operating characteristics when using ε_k as it results from the analysis of the aftershocks, i.e., $\eta_k = m_k/10$, where the denominator 10 has been selected so that $\eta_k < 1$ [cf. Eq. (29)], where $m_k(\geqslant 2.0)$ is the magnitude reported in the Southern California Earthquake Catalog for the kth aftershock of the June 28, 1992, Landers and of the October 16, 1999, Hector Mine earthquakes during the Omori regimes estimated in Ref. [58]. Following Ref. [7], we considered the aftershocks that occurred within a square region of $1.1^0 \times 1.1^0$ and $1.0^0 \times 1.0^0$ centered at the epicenter of the Landers and the Hector Mine earthquakes, respectively. For the sake of comparison, we also plot in each ROC graph the results obtained by the same prediction algorithm when applied to *randomly* shuffled copies of the original aftershock sequence $\{m_k\}$. We observe that ε_k has statistically significant predictive power associated with the (true time) order k of aftershocks and hence with natural time.

Let us finally, comment on the fact that real earthquakes—which by definition are highly localized events in space and time—are a result of complex interactions between the elements making up the crust of the Earth together with criticality (e.g., see Refs. [44,46,47]), and thus are much more complex phenomena than those described by the coherent-noise model. The latter, as mentioned, consists of noninteracting agents which are driven by a coherent noise. According to our opinion, it is the fact that the coherent-noise model exhibits similar temporal structures (i.e., aftershock sequences) with real earthquakes that is responsible for the statistically significant predictive power of ε_k in the case of aftershocks which has been discussed in the previous paragraph.

V. CONCLUSIONS

The threshold distribution function $p^{(k)}_{\text{thres}}(x)$ of the coherent-noise model for the case of infinite number of agents after the occurrence of the kth avalanche was studied. This is a piecewise function with a finite number of steps n_k [cf. Eq. (11)]. An analytic expression has been obtained for the size distribution function of the next avalanche [cf. Eq. (26)]. This enables the estimation of the expected size of the next avalanche $\mathscr{E}(S_{k+1})$ [e.g., for the case of exponentially distributed stresses η_k, see Eq. (28)]. The possibility of using $\mathscr{E}(S_{k+1})$ or n_k as a decision variable for the prediction of the size S_{k+1} of the next avalanche was investigated. The results obtained point to a tentative prediction scheme for real earthquake aftershock data.

APPENDIX A: DERIVATION OF $\mathscr{E}(S)$ IN THE CASE OF THE EXPONENTIAL DISTRIBUTION

When $p_{\text{stress}}(\eta) = \exp(-\eta/\sigma)/\sigma$, Eq. (27)—in view of Eq. (26)—reads

$$\mathscr{E}(S_{k+1}) = \sum_{l=0}^{n_k} \int_{\alpha_l b_l^{(k)} - \beta_l}^{\alpha_l b_{l+1}^{(k)} - \beta_l} \frac{S_{k+1} \exp\left(-\frac{S_{k+1}+\beta_l}{\sigma\alpha_l}\right)}{\sigma\alpha_l} \times dS_{k+1} + \exp(-1/\sigma). \tag{A1}$$

Direct evaluation of the integrals leads to

$$\int_{\alpha_l b_l^{(k)}-\beta_l}^{\alpha_l b_{l+1}^{(k)}-\beta_l} \frac{S_{k+1}\exp\left(-\frac{S_{k+1}+\beta_l}{\sigma\alpha_l}\right)}{\sigma\alpha_l} dS_{k+1}$$

$$= \left(\alpha_l b_l^{(k)} - \beta_l + \sigma\alpha_l\right)\exp\left(-\frac{b_l^{(k)}}{\sigma}\right)$$

$$- \left(\alpha_l b_{l+1}^{(k)} - \beta_l + \sigma\alpha_l\right)\exp\left(-\frac{b_{l+1}^{(k)}}{\sigma}\right). \quad \text{(A2)}$$

By substituting Eq. (A2) into Eq. (A1), rearranging the terms, and using the identity

$$\beta_l - \beta_{l-1} = b_l^{(k)}(\alpha_l - \alpha_{l-1}) \quad \text{(A3)}$$

that holds due to Eqs. (25), we finally obtain Eq. (28) of the main text.

APPENDIX B: THE SETS OF SUCCESSIVE EXTREMA

The sets E_k of successive extrema are defined [51] as follows: E_0 equals the empty set. Each E_k is obtained by the procedure described below for k times. Select a random number η_k from a given probability density function $f(\eta)$ and compare it with all the members of E_{k-1}. In order to construct the set E_k, we discard from the set E_{k-1} all its members that are smaller than η_k and furthermore include η_k. Thus, $E_k \neq \emptyset$ for *all* $k > 0$ and E_k is a finite set of real numbers whose members are always larger or equal to η_k. Moreover,

$$\max[E_k] \geqslant \max[E_{k-1}]. \quad \text{(B1)}$$

The increase of the cardinality $\varepsilon_k \equiv |E_k|$ of these sets is at the most 1, but its decrease may be as large as $\varepsilon_k - 1$. This reflects an asymmetry if ε_k is considered as time series with respect to the *natural* number k. Such an asymmetry is reflected in Fig. 3 where instead of ε_k, we depict n_k of the coherent-noise model which equals—due to Eqs. (12) and (17)—to ε_k as long as all η_l, $l = 1,2,\ldots,k$ are smaller than unity.

[1] S. Havlin, S. V. Buldyrev, A. L. Goldberger, R. N. Mantegna, S. M. Ossadnik, C. K. Peng, M. Simons, and H. E. Stanley, Chaos, Solitons Fractals **6**, 171 (1995).

[2] C. K. Peng, S. V. Buldyrev, A. L. Goldberger, S. Havlin, R. N. Mantegna, M. Simons, and H. E. Stanley, Physica A **221**, 180 (1995).

[3] H. E. Stanley, S. V. Buldyrev, A. L. Goldberger, S. Havlin, C. K. Peng, and M. Simons, Physica A **273**, 1 (1999).

[4] C. K. Peng, S. Havlin, H. E. Stanley, and A. L. Goldberger, Chaos **5**, 82 (1995).

[5] M. E. J. Newman, Proc. R. Soc. London, Ser. B **263**, 1605 (1996).

[6] J. B. Rundle, D. L. Turcotte, R. Shcherbakov, W. Klein, and C. Sammis, Rev. Geophys. **41**, 1019 (2003).

[7] R. Shcherbakov, D. L. Turcotte, and J. B. Rundle, Geophys. Res. Lett. **31**, L11613 (2004).

[8] J. R. Holliday, J. B. Rundle, D. L. Turcotte, W. Klein, K. F. Tiampo, and A. Donnellan, Phys. Rev. Lett. **97**, 238501 (2006).

[9] S. Lennartz, A. Bunde, and D. L. Turcotte, Phys. Rev. E **78**, 041115 (2008).

[10] A. S. Balankin, D. Morales Matamoros, J. Patiño Ortiz, M. Patiño Ortiz, E. Pineda León, and D. Samayoa Ochoa, EPL **85**, 39001 (2009).

[11] M. J. Aschwanden, R. W. Nightingale, T. D. Tarbell, and C. J. Wolfson, Astrophys. J. **535**, 1027 (2000).

[12] C. E. Parnell and P. E. Jupp, Astrophys. J. **529**, 554 (2000).

[13] D. Hughes, M. Paczuski, R. O. Dendy, P. Helander, and K. G. McClements, Phys. Rev. Lett. **90**, 131101 (2003).

[14] G. Nigro, F. Malara, V. Carbone, and P. Veltri, Phys. Rev. Lett. **92**, 194501 (2004).

[15] V. Frette, K. Christensen, A. Malthe-Sørenssen, J. Feder, T. Jøssang, and P. Meakin, Nature (London) **379**, 49 (1996).

[16] C. M. Aegerter, R. Gunther, and R. J. Wijngaarden, Phys. Rev. E **67**, 051306 (2003).

[17] K. A. Lőrincz and R. J. Wijngaarden, Phys. Rev. E **76**, 040301 (2007).

[18] P. A. Varotsos, N. V. Sarlis, and E. S. Skordas, Phys. Rev. E **67**, 021109 (2003); **68**, 031106 (2003); Chaos **19**, 023114 (2009).

[19] P. Bak, *How Nature Works* (Copernicus, New York, 1996).

[20] H. J. Jensen, *Self-Organized Criticality: Emergent Complex Behavior in Physical and Biological Systems* (Cambridge University Press, New York, 1998).

[21] D. Sornette, *Critical Phenomena in Natural Science*, 2nd ed. (Springer-Verlagw, Berlin Heidelberg, 2004).

[22] P. Bak, C. Tang, and K. Wiesenfeld, Phys. Rev. Lett. **59**, 381 (1987).

[23] A. Garber, S. Hallerberg, and H. Kantz, Phys. Rev. E **80**, 026124 (2009).

[24] A. Garber and H. Kantz, Eur. Phys. J. B **67**, 437 (2009).

[25] P. Bak, C. Tang, and K. Wiesenfeld, Phys. Rev. A **38**, 364 (1988).

[26] O. Ramos, E. Altshuler, and K. J. Måløy, Phys. Rev. Lett. **102**, 078701 (2009).

[27] M. E. J. Newman and K. Sneppen, Phys. Rev. E **54**, 6226 (1996).

[28] K. Sneppen and M. Newman, Physica D **110**, 209 (1997).

[29] C. Wilke, S. Altmeyer, and T. Martinetz, Physica D **120**, 401 (1998).

[30] U. Tirnakli and S. Abe, Phys. Rev. E **70**, 056120 (2004).

[31] A. Celikoglu, U. Tirnakli, and Silvio M. Duarte Queirós, Phys. Rev. E **82**, 021124 (2010).

[32] E. Ergun and U. Tirnakli, Eur. Phys. J. B **46**, 377 (2005).

[33] P. Varotsos and K. Alexopoulos, Tectonophysics **110**, 73 (1984); **110**, 99 (1984).

[34] P. Varotsos and M. Lazaridou, Tectonophysics **188**, 321 (1991).

[35] P. Varotsos, K. Alexopoulos, and M. Lazaridou, Tectonophysics **224**, 1 (1993).

[36] S. L. Pepke and J. M. Carlson, Phys. Rev. E **50**, 236 (1994).

[37] Y. Huang, H. Saleur, C. Sammis, and D. Sornette, Europhys. Lett. **41**, 43 (1998).

[38] C. G. Sammis and S. W. Smith, Pure Appl. Geophys. **155**, 307 (1999).

[39] N. V. Sarlis, E. S. Skordas, M. S. Lazaridou, and P. A. Varotsos, Proc. Japn. Acad., Ser. B **84**, 331 (2008).

[40] S. Uyeda and M. Kamogawa, Eos Trans. Am. Geophys. Union **89**, 363 (2008).
[41] S. Uyeda, M. Kamogawa, and H. Tanaka, J. Geophys. Res. **114**, B02310 (2009).
[42] S. Uyeda and M. Kamogawa, Eos Trans. Am. Geophys. Union **91**, 163 (2010).
[43] N. V. Sarlis, E. S. Skordas, and P. A. Varotsos, EPL **91**, 59001 (2010).
[44] P. A. Varotsos, N. V. Sarlis, E. S. Skordas, S. Uyeda, and M. Kamogawa, EPL **92**, 29002 (2010).
[45] P. Varotsos, N. Sarlis, and E. Skordas, EPL **96**, 59002 (2011).
[46] P. A. Varotsos, N. V. Sarlis, and E. S. Skordas, *Natural Time Analysis: The New View of Time. Precursory Seismic Electric Signals, Earthquakes and other Complex Time-Series* (Springer-Verlag, Berlin Heidelberg, 2011).
[47] P. Varotsos, N. V. Sarlis, E. S. Skordas, S. Uyeda, and M. Kamogawa, Proc. Natl. Acad. Sci. USA **108**, 11361 (2011).
[48] P. A. Varotsos, N. V. Sarlis, and E. S. Skordas, Practica of Athens Academy **76**, 294 (2001).
[49] P. A. Varotsos, N. V. Sarlis, and E. S. Skordas, Phys. Rev. E **66**, 011902 (2002).
[50] N. Sarlis, E. Skordas, and P. Varotsos, EPL **96**, 28006 (2011).
[51] N. V. Sarlis, E. S. Skordas, and P. A. Varotsos, EPL **87**, 18003 (2009).
[52] F. Caruso and H. Kantz, Eur. Phys. J. B **79**, 7 (2011).
[53] V. I. Keilis-Borok and I. M. Rotwain, Phys. Earth Planet. Inter. **61**, 57 (1990).
[54] V. I. Keilis-Borok and V. G. Kossobokov, Phys. Earth Planet. Inter. **61**, 73 (1990).
[55] T. Fawcett, Pattern Recogn. Lett. **27**, 861 (2006).
[56] Z. Olami, Hans Jacob S. Feder, and K. Christensen, Phys. Rev. Lett. **68**, 1244 (1992).
[57] N. Sarlis, E. Skordas, and P. Varotsos, Tectonophysics **513**, 49 (2011).
[58] S. Abe and N. Suzuki, Physica A **332**, 533 (2004).